Ecotoxicology and Environmental Safety 322 (2026) 120532

Contents lists available at ScienceDirect

Ecotoxicology and Environmental Safety

journal homepage: www.elsevier.com/locate/ecoenv

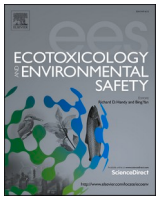

Impact of a pristine versus gastric acid-treated low-density polyethylene in a human epithelial colorectal adenocarcinoma (Caco-2) cell line

Inés Tejeda [a], Nelly D. Saenen [a], Margo S. Witters [a], Wouter Marchal [b], An Hardy [c], Jacco J. Briedé [d], Frank G.A.J. Van Belleghem [a,e], Karen Smeets [a,*]

[a] Centre for Environmental Sciences, Hasselt University, Agoralaan Building D, Diepenbeek 3590, Belgium
[b] Analytical & Circular Chemistry, Institute for Materials Research IUMAT, Hasselt University, Agoralaan Building D, Science Tower, Diepenbeek 3590, Belgium
[c] Design and Synthesis of Inorganic Materials (DESINe), Institute for Materials Research IUMAT, Hasselt University, Agoralaan Building D, Science Tower, Diepenbeek 3590, Belgium
[d] Department of Translational Genomics, Maastricht University, Universiteitssingel 50, 6229ER Maastricht and Research Institute for Oncology and Reproduction (GROW), Maastricht, the Netherlands
[e] Department of Environmental Sciences, Faculty of Science, Open Universiteit, Valkenburgerweg 177, Heerlen 6419 AT, the Netherlands

ARTICLE INFO

Keywords:
Physico-chemical characterization
LDPE
Microplastics
In vitro
Mitochondria
ROS

ABSTRACT

An increasing number of studies report the presence and accumulation of micro- and nanoplastics (MNPs) in the human body. After ingestion, MNPs undergo weathering by gastric and intestinal fluids that modify their physicochemical properties. Although these changes can influence biological responses, their impact remains understudied, forming the foundation of this research. We investigated how a simplified chemical weathering model of simulated gastric fluid exposure alters the physicochemical properties of environmentally relevant microplastics and how these changes influence their subsequent effects on a human epithelial colorectal adenocarcinoma (Caco-2) cell line. We focused on Low-Density Polyethylene (LDPE) due to its widespread use in agriculture and food packaging, as well as its status as one of the most widely produced plastic polymers. Particle properties changed after artificial stomach acid (ASA) treatment, including metal leaching, surface modifications, stronger redox-inducing potential, and increased floatability. These changes in the particles' characteristics were reflected in the observed effects, with ASA-treated particles producing more pronounced alterations in mitochondrial network features, including increased mitochondrial fusion and a larger mitochondrial footprint. No internalization was observed in any of the cases, with membrane integrity (5-CFDA,AM) disrupted after exposure to pristine and ASA-treated particles, regardless of the underlying mechanistic pathways. In summary, our findings show that ASA-treated microplastics differ in redox-inducing potential, which can influence cellular metabolism regardless of cellular uptake. This suggests that indirect changes after ASA treatment may represent an underestimated part of microplastic toxicity after ingestion.

1. Introduction

Microplastics (MPs), defined as particles smaller than 5 mm (Hartmann et al., 2019), are categorized into primary and secondary MPs based on their origin. Primary MPs, artificially designed to specific sizes, are commonly found in household and personal care products (Wu et al., 2019). Secondary MPs arise from the degradation of larger plastics (Kershaw and Rochman, 2015; Wu et al., 2019) through various processes, including UV radiation, mechanical degradation, thermal effects, or biological weathering (Alimi et al., 2022). MPs have been detected in tap and bottled water, various foods, including honey and fish (Barboza et al., 2018; Kosuth et al., 2018; Liebezeit and Liebezeit, 2013). Consequently, ingestion is considered one of the major routes of MPs exposure in humans (Prata et al., 2020), which is supported by the frequent detection of MPs in human stool samples (Ho et al., 2022; Refosco et al., 2025; Song et al., 2025). Polyethylene (PE), polypropylene (PP), and polyethylene terephthalate (PET) are among the most commonly detected polymers, reflecting their widespread use in food packaging and consumer products. MPs were detected in the majority of the samples analyzed (>90%), with reported concentrations of 54.7 μg/g or 1–138.9 particles/g (Ho et al., 2022; Refosco et al., 2025; Song et al., 2025). Despite this, a meta-analysis of Caco−2 cell studies

* Corresponding author.
E-mail address: karen.smeets@uhasselt.be (K. Smeets).

https://doi.org/10.1016/j.ecoenv.2026.120532
Received 4 March 2026; Received in revised form 30 June 2026; Accepted 18 July 2026
Available online 23 July 2026

found that most toxicological studies have been conducted at higher concentrations (>100 μg/ml), suggesting a bias toward higher, less environmentally relevant concentrations (Ferreira et al., 2024).

At the same time, most *in vitro* studies focus on pristine spherical polystyrene (PS) particles (Fournier et al., 2021; Hirt and Body-Malapel, 2020; Völkl et al., 2022), whereas real-life particles are more heterogeneous in shape and composition. Weathering processes such as UV irradiation, mechanical abrasion, or biodegradation modify particle surface characteristics and additive release (Alimi et al., 2022; Zhang et al., 2021), potentially influencing their biological activity. Following ingestion, exposure to gastric and intestinal fluids may further induce polymer-dependent transformations affecting chemical release, particle agglomeration, and cellular interactions (Prabhu et al., 2024). For example, simulated digestion has been reported to promote particle agglomeration and reduce uptake in Caco−2 cells without substantially altering cytotoxicity (Paul et al., 2024), underscoring the need to investigate these processes across a broader range of polymers. However, toxicological findings on weathered particles are inconsistent, with studies reporting both increased stress and negligible differences compared to pristine particles (Bond et al., 2022; Dusza et al., 2022; Völkl et al., 2022). These discrepancies suggest that biological responses are strongly dependent on particle characteristics and specific weathering conditions applied (Bond et al., 2022; Völkl et al., 2022), yet the underlying mechanisms remain insufficiently understood. (Liu et al., 2024; Paul et al., 2024). Mitochondrial responses, including elevated reactive oxygen species (ROS) production, disruption of mitochondrial membrane potential, and activation of mitochondrial quality-control mechanisms such as mitophagy, have increasingly been reported following MP exposure (Banerjee and Shelver, 2021; Hu and Palić, 2020; Li et al., 2023). However, it remains unclear to what extent these effects are driven by physicochemical changes.

In the context of the abovementioned research gaps, this study aimed to investigate the effects of larger irregular MPs, which are not readily uptaken by cells, before and after treatment with a simplified gastric chemical weathering model, using the human epithelial colorectal adenocarcinoma Caco−2 cell line as an *in vitro* model of the human intestinal barrier. The Caco−2 cell line was selected because it is a widely characterized and used model for intestinal absorption studies (Angelis and Turco, 2011; Bredeck et al., 2022; Ferreira et al., 2024), allowing comparison with previous studies on particles and chemical compounds. Its use also aligns with the REACH regulatory framework, which explicitly promotes the use of non-animal methods (European Parliament and Council of the European Union, 2006), and the 3Rs principles (Replacement, Reduction, Refinement), for chemical safety assessment (EFSA's Scientific Committee promotes alternatives to animal testing, EFSA, 2009). Artificial stomach acid (ASA) was used as a controlled first step toward unraveling gastrointestinal weathering. By focusing on selected chemical parameters, this approach reduced variability from concurrent enzymatic, mechanical, and microbial processes, enabling observed effects to be more directly linked to specific physicochemical changes. Cellular responses were assessed across a broad concentration range, with concentrations $\leq$ 10 μg/ml included to reflect more environmentally and physiologically relevant acute exposure conditions, given that most current in vitro studies employ substantially higher exposure concentrations. (Ferreira et al., 2024). Endpoints included cell viability, particle-cell interactions, oxidative reactivity, and mitochondrial network features. Low-density polyethylene (LDPE) was selected due to its widespread usage (Barboza et al., 2019; El-Sherif et al., 2022; Emblem, 2012; Geyer et al., 2017) and is among the most commonly used packaging plastics in the EU (Lyshtva et al., 2025; Torkelis et al., 2024). By combining physicochemical characterization with assessments of membrane integrity, oxidative reactivity, and mitochondrial network dynamics within the same experimental framework, this study provides a more integrated understanding of how weathering-induced changes in particle properties translate into biological responses.

2. Materials and methods

2.1. Microplastics

Samples of commercially available plastic sheets of polypropylene (PP), nylon (PA), and Polyvinyl chloride (PVC) purchased online via www.kunststofshop.nl and a plastic bottle of polyethylene terephthalate (PET) were manually cut into 5 × 5 mm pieces and subsequently cryomilled using MM400 Mixer Mill with the stainless-steel grinding jar 50 ml and stainless-steel grinding ball 25 mm accessories (Retsch GmbH, Haan, Germany). For cryomilling, the plastic squares were placed in the jar with the grinding ball and submerged in liquid nitrogen until the equilibrium temperature was reached. Milling was conducted for 1.5 min at 30 Hz. The process was repeated four times. Polybutylene terephthalate (PBT) powder, LDPE [< 50 μm white ($LDPE_{<50}$), 50–250 μm black ($LDPE_{50–250,black}$), 50–100 μm white ($LDPE_{50–100,white}$)], and polymethylmethacrylate (PMMA) 6 μm spheres were kindly provided by Dutch State Mines (DSM, Haarlem, Netherlands), Wageningen University (Qi et al., 2018), and Institute for Materials Research IUMAT (UHasselt), respectively.

The $LDPE_{<50}$ was further subdivided into size fractions by filtration (KNF, Sursee, Switzerland) using Merck Nylon Net (Darmstadt, Germany) filters with pore sizes of 80, 41, and 30 μm. A suspension of $LDPE_{<50}$ at 10 mg/ml was prepared in sterile Milli-Q water (Puranity PU 15 UV/UF, VWR, Radnor, Pennsylvania, USA) and filtered through filters with increasingly smaller pore sizes. The particles captured on the 30 μm pore-size filters were recovered with filtered Milli-Q water by inverse flushing and dried in an oven (Sheldon Manufacturing Inc., Cornelius, Oregon, USA) at 56 °C.

Artificial stomach acid (ASA) was prepared by dissolving in 50 ml of Milli-Q water 0.65 g/L of glucose, 0.40 g/L of $CaCl_2$, 0.288 g/L of NaH_2PO_4 (Merck KGaA, Darmstadt, Germany), 0.8252 g/L of NaCl, and 78 mM of HCl (VWR, Radnor, Pennsylvania, USA). Subsequently, NaOH (UCB, Brussels, Belgium) was used to adjust the pH to 2.5, which represents a physiologically relevant gastric acidity within the commonly reported human stomach range (pH 1.5–2.5; Kennedy and Chang, 2020). The prepared ASA solution was stored for up to 1 month in plastic containers (screw cap tube 15 ml, (LxØ): 120 × 17 mm, PP, with print, Sarstedt AG & Co. KG, Nümbrecht, Germany) to limit the effect of the container on the ASA. Immediately before cell exposure, 5 mg/ml microplastics were incubated within the ASA for 30 min at 37 °C in an ISOtemp GDP 05 water bath (Fisher Scientific, Hampton, New Hampshire, USA). An exposure duration of 30 min was selected to reflect physiologically relevant gastric residence times for liquids, for which water exhibits a half-emptying time of approximately 14 min in healthy adults (Ziessman et al., 2009). This simplified system was designed as a gastric chemical weathering model focused on the effects of acidity and ionic composition, with digestive enzymes such as pepsin excluded.

From now on, the original LDPE < 50 μm white will be referred to as $LDPE_{<50}$, the size fraction of LDPE will be referred to as $LDPE_{30–41}$, and their ASA-treated counterparts will be referred to as $LDPE_{<50}$-ASA and $LDPE_{30–41}$-ASA.

2.2. Physicochemical characterization

2.2.1. Scanning electron microscopy (SEM)

A suspension of MPs was prepared in Propanol:Milli-Q water (Sigma-Aldrich, Burlington, Massachusetts, USA) at a 1:1 ratio, with concentrations ranging from 500 μg/ml to 1 mg/ml. The samples were prepared on aluminium pin stubs Ø12.7 (Micro to Nano, Haarlem, Netherlands) using Ø12mm high purity conductive double-sided adhesive carbon tabs (Micro to Nano, Haarlem, Netherlands) and dried in an oven (Sheldon Manufacturing Inc, Cornelius, Oregon, USA) at 56 °C inside a partially open single pin mount storage and transport tube (Micro to Nano, Haarlem, Netherlands).

The MPs were imaged using the desktop Scanning Electron

Microscope Phenom ProX, equipped with the Phenom ProSuite software (Thermo Fisher Scientific™, Waltham, Massachusetts, USA), at magnifications ranging from 190x to 810x. The MPs' size distributions were determined using the image-processing program ImageJ 1.53k, measuring the Feret distance between the smallest (min) and the longest distance between opposite sides (max) of each particle. Two independent measurements were conducted for the preliminary evaluation of PVC, PP, PET, PA, and PBT, with a total of 200 MPs quantified. To evaluate the efficacy of $LDPE_{<50}$ filtering and to investigate the potential differences between pristine and ASA-treated materials, three independent measurements were carried out to assess the size distribution of $LDPE_{<50}$, $LDPE_{30–41,}$ and $LDPE_{30–41}$-ASA, resulting in a cumulative sample size of 375 particles for each condition.

2.2.2. X-ray fluorescence (XRF)

LDPE composition was studied by elemental analysis using a Shimadzu energy-dispersive EDX8100P equipped with an SDD detector and a 50 kV X-ray generator with a Rh target. Measurements are performed in the semi-quantitative Quant-FP mode under a He atmosphere. The $LDPE_{<50}$ samples were analyzed in powder cups shielded with Ultralene® Window Film, 0.16 mil (4 μm) Thick (SPEX Sample Prep, Metuchen, New Jersey, USA).

2.2.3. Gas chromatography-mass spectrometry (GC-MS)

Additives were extracted from the $LDPE_{<50}$ powder sample by Soxhlet extraction. 5.016 g LDPE (< 100–50 μm) sample was weighed into an extraction thimble and placed in the Soxhlet extractor using a 50/ 50 solvent mixture of dichloromethane/hexane. The extraction was carried out for 6 h under continuous heating and reflux in the Soxhlet apparatus. After completion, the extract volume was first reduced using a rotary evaporator and then further concentrated by nitrogen blowdown to a final volume of 1 ml. Prior to analysis, the extract was passed through a 0.45 μm PTFE filter to remove any remaining particulates. The extracted sample was analyzed by gas chromatography-mass spectrometry (GC-MS).

The GC–MS analysis was performed on a Trace 1310 gas chromatograph (Thermo Scientific, USA) equipped with a DB−5MS capillary column (30 m length, 0.25 mm I.D., film thickness 0.25 μm, Agilent Technologies, USA) and coupled to an ISQ LT single quadrupole mass spectrometer (Thermo Scientific, USA). A sample volume of 1 μl was injected using a 1/100 split. The oven temperature was set to 50 °C upon injection and ramped to 330 °C at 15 °C/min, with a final hold time of 9 min. The injection port and MS transfer line were both set at 280 °C. Helium was used as the carrier gas and the flow rate was set at 1.2 ml/min. The mass spectrometer was operated in electron ionization mode at 70 eV, with a source temperature of 250 °C, a mass range of 50–700 *m/z*, and a scan time of 0.1 s.

Data processing was performed using Chromeleon 7.3 (Thermo Scientific, USA).

2.2.4. Differential scanning calorimetry (DSC)

Differential Scanning Calorimetry measurements were carried out on a DSC Q200 (TA Instruments), using approximately 4 mg portions in Al-sample pans. The samples were cycled at 20 °C/min for 2 repetitive heating-cooling cycles up to 160 °C. The melting enthalpies were determined by peak integration using a linear baseline.

2.2.5. Fourier transform infrared spectroscopy (FTIR)

To understand the changes in the surface of the ASA-treated particles, $LDPE_{<50}$ and $LDPE_{<50}$-ASA were measured with FTIR. Measurements are carried out on a Bruker Invenio S in attenuated total reflection (ATR) mode. Spectra are collected between 4,000 and 400 cm^{-1} with a spectral resolution of 4 cm^{-1}, accumulating 32 scans per spectrum.

2.2.6. Inductively coupled plasma atomic emission spectrometry (ICP-AES)

The composition of the leachate after the ASA treatment of $LDPE_{<50}$ was analyzed by ICP-AES. The samples were incubated in ASA at 100 mg/ml for 30 min at 40 ºC. The sample was centrifuged, and the aliquots were analyzed on a Perkin Elmer Optima 8300 DV spectrometer after dilution (factor 1:5) and filtration. Average values of 3 consecutive measurements are reported, and a 5 QC sample is included for each reported element. The results were corrected to an LDPE blank.

2.2.7. Electron spin resonance (ESR) spectroscopy

The Reactive Oxygen Species (ROS) formation capacity of the $LDPE_{<50}$, PA, PET, PBT, PP, and PVC was tested via Electron Spin Resonance (ESR) spectroscopy in combination with a spin trapping technique employing 2,2-Dimethyl−3,4-dihydro−2H-pyrrole 1-oxide (DMPO). 10 mg of the plastics were incubated in a warm water bath (Salm & Kipp BV, Breukelen, The Netherlands) at 37.5 ºC in the ASA or Milli-Q water for 30 or 60 min using DMPO (100 mM) for hydroxyl ($OH^{\cdot}$) and superoxide ($O_2^{\cdot-}$) radical entrapment. The suspensions were transferred to glass capillary tubes (100 μl, Brand AG Wertheim, Germany) and measured at room temperature on a Bruker EMX 1273 spectrometer equipped with an ER 4119HS high-sensitivity cavity and a 12 kW power supply operating at X-band frequencies with a modulation frequency of 100 kHz. Instrumental conditions for the recorded spectra were: magnetic field: 3490 G; scan range: 60 G; modulation amplitude: 1 G; receiver gain: 1 × 105; microwave frequency: 9.85 GHz; power: 50 mW; time constant: 40.96 ms; scan time: 20.97 s; number of scans: 30. Spectra were quantified by peak surface measurements using the WIN-EPR spectrum manipulation program (Bruker, Germany). As controls, ASA, Milli-Q, and Milli-Q water with the plastics, incubating them for 30 or 60 min, were measured. The experiments and controls were conducted with ASA stored in plastic (ASAp) and glass (ASAg) containers to determine whether container type affected the measurements.

In the preliminary screening, a single measurement was performed for all conditions. For $LDPE_{<50}$ five independent measurements were acquired for the controls, while two to five independent measurements were taken for each experimental condition. The second peak of the ROS pattern was measured in all samples.

2.3. Cell culture conditions and experimental set-up

Caco−2 cells were selected as they differentiate into an intestinal epithelial-like monolayer and are widely used to study intestinal absorption, barrier interactions, and responses to ingested contaminants. Caco−2 cells were obtained from the American Type Culture Collection (HTB37™, LGC Standards, Wesel, Germany). The maintenance culture medium consisted of Dulbecco's Modified Eagle Medium Gluta-Max™ (DMEM) supplemented with 10% of heat-inactivated fetal bovine serum, 1% non-essential amino acids, 2.5% HEPES, and 0.1% gentamicin (Gibco™, Fisher Scientific, Brussels, Belgium). After thawing, Caco−2 cells were initially cultivated in 25 cm^2 flasks for one passage before being transferred to 75 cm^2 flasks (Greiner, Sigma-Aldrich, Darmstadt, Germany) for maintenance. The cells were cultivated at 5% CO_2 and 37 ºC, with the medium being refreshed twice a week. Subculturing was performed before reaching 70% confluence using Phosphate-Buffered Saline (PBS, Fisher Scientific, Brussels, Belgium) and Trypsin-EDTA 0.05% (Gibco™, Fisher Scientific, Brussels, Belgium). Cells with passage numbers ranging from 30 to 38 were used in the experiments, which is in the range reported to reduce variability (Briske-Anderson et al., 1997; Kus et al., 2023).

For the experimental setup, the cells were seeded either in 96-well plates (Greiner, Sigma-Aldrich, Germany) at a density of 1.35 × 10^4 cells/cm^2 for cell viability assays or in 8-well IBIDI chambers (Ibidi GmbH, Gräfelfing, Germany) at a density of 3 × 10^4 cells/cm^2 until a monolayer was established. Exposure was carried out in Dulbecco's Modified Eagle Medium™ containing 10% of heat-inactivated fetal bovine serum, 1% non-essential amino acids, and 1% antibiotics (10,000 μg/ml streptomycin and 10,000 IU/ml penicillin) or in Dulbecco's Modified Eagle Medium™ phenol red-free without any

supplements for live confocal imaging. All washes were performed with Dulbecco's phosphate-buffered saline (dPBS) containing Mg^{2+} and Ca^{2+} (Gibco™, Fisher Scientific, Brussels, Belgium).

2.4. Cell viability

Cell viability was assessed using the combination of Alamar Blue (AB, Invitrogen™) and 5-Carboxyfluorescein Diacetate, Acetoxymethyl Ester (5-CFDA, AM, Invitrogen™). The procedure followed is based on Schirmer et al. (1997) with some modifications. 5-CFDA, AM stock solution was prepared in Dimethyl sulfoxide (DMSO, Merck) in a concentration of 4 mM and kept frozen at −20ºC until use. AB was bought in a ready-to-use solution and refrigerated at 4ºC until use. The cells were exposed to a range (1–150 μg/ml) of $LDPE_{30–41}$ or $LDPE_{30–41}$-ASA for 24 h. The wells were emptied and washed with warm dPBS. Then, an aliquot of 120 μl was added to a solution prepared with DMEM without phenol red 5% AB (v/v) and 4 μM 5-CFDA, AM, and incubated for 30 min (37 ºC, 5% CO_2, dark). Fluorescence of AB (Ex/Em: 530/595 nm) and 5-CFDA, AM (Ex/Em: 493/541 nm) was measured using FLUOstar Omega Microplate Reader (BMG Labtech, Ortenberg, Germany) in arbitrary units. Background fluorescence from wells without cells was subtracted in all wells. Four independent experiments were performed, with 3–6 biological replicates per experiment. Parallel to the cell viability assays, a cell-free interference assay was conducted, following the same steps and concentrations described in this protocol to measure any particles left in the wells after the washes.

To determine whether MPs could interfere with our assays, we conducted an experiment measuring the MP signal after exposure to Alamar Blue and 5-CFDA, AM, using the same concentrations and plastics as in the viability assays. Six replicates were aliquoted in a 96-well plate, incubated for 30 min (37 ºC, 5% CO_2, dark), and the fluorescence of AB (Ex/Em: 530 /595 nm) and 5-CFDA, AM (Ex/Em: 493 / 541 nm) was measured using FLUOstar Omega Microplate Reader. After the measurements, 15 μl of the samples were recovered from the 150 μg/ml exposure concentration and the control conditions and imaged using CLSM (LSM900) at 40x magnification using the same Ex/Em as in the plate reader for qualitative assessment.

2.5. Visualization of uptake and effects using confocal microscopy

2.5.1. LDPE uptake

$LDPE_{30–41}$ was stained with the lipophilic stain Nile Red (Abcam, Cambridge, United Kingdom). Staining was performed according to the Prata et al. (2019) with the following changes: the plastic was stained with a concentration of 2 μg/ml at 70 ºC for 3.5 h in a glass bottle, followed by filtration with a Merck Nylon Net filter with a pore size of 10 μm and continuous rinsing with filtered Milli-Q for 1 min. The particles were recovered from the filter with filtered Milli-Q, dried overnight at 70 ºC in the dark, and resuspended at 1 mg/ml in filtered, sterilized Milli-Q.

The immunofluorescent dye Molecular Probes™ CellMask™ Green Plasma Membrane Stain (Ex/Em: 535/522, Invitrogen, Fisher Scientific, Brussels, Belgium) was used to qualitatively assess Nile Red-stained $LDPE_{30–41}$ uptake. Before exposure, the culture medium was removed, and cells were washed twice with warm dPBS ($+Ca^{2+}$, $+Mg^{2+}$). After exposure to 500 μg/ml of Nile Red-stained $LDPE_{30–41}$ and Nile Red-stained $LDPE_{30–41}$-ASAg for 24 h in phenol-free DMEM medium, the cells were immediately stained with a 0.5x concentration of Molecular Probes™ CellMask™ Green Plasma Membrane Stain in the exposure medium for 10 min at 37 °C in darkness. Live imaging was performed using Confocal Laser Scanning Microscopy (CLSM, LSM900, Zeiss, Zaventem, Belgium) equipped with high-power diode lasers at 405, 488, 514, and 633 nm and mounted on an inverted laser-scanning microscope (Axio Observer Z1/7, Zeiss, Zaventem, Belgium). For each condition, 20 particles were manually assessed for floatability by taking six z-stack images at 40x magnification (Ex/Em: 577/603 nm, $LDPE_{30–41}$(-ASA); Ex/Em: 535/522 nm, plasma membrane stain). Qualitative images were captured using the same setup, with an exposure concentration of 100 μg/ml due to the limited availability of the $LDPE_{30–41}$ sample.

2.5.2. Analysis of mitochondrial network morphology

Given that pristine MPs have the potential to impact mitochondrial function in Caco−2 cells (Saenen et al., 2023; Wu et al., 2019), we assessed the mitochondrial network morphology using MitoTracker Red CMXRos (Invitrogen™, Thermo Fisher Scientific, Waltham, Massachusetts, USA) after 24 h of exposure of the Caco−2 monolayer to 0, 10, and 100 μg/ml $LDPE_{30–41}$ or $LDPE_{30–41}$-ASAg. The cells were seeded in 8-well IBIDI chambers and cultured until a monolayer was formed. After exposure, the culture medium was removed, and the cells were washed twice with warm dPBS ($+Ca^{2+}$, $+Mg^{2+}$). The cells were incubated with 300 μl of MitoTracker Red CMXRos (250 nM) diluted in warm PBS for 45 min at 37 ºC and 5% CO_2 in darkness. After being rinsed twice with warm PBS, they were immediately imaged. Live imaging was performed using a CLSM (LSM900, Zeiss, Zaventem, Belgium) equipped with high-power diode lasers at 405, 488, 514, and 633 nm, mounted on an inverted laser-scanning microscope (Axio Observer Z1/7, Zeiss, Zaventem, Belgium). The images were obtained at 40x and Ex/Em: 579/599 nm. For each condition, a tile scan (300 μm x 600 μm) was recorded using ZEN blue 3.1 software (Zeiss, Zaventem, Belgium) with the same settings across all experiments, and the images were exported with a fixed weight applied to the low-level signals. Three independent experiments were performed for all the conditions, each with 3–4 images per condition. In each condition, 5–7 cells were randomly selected from the same plane in each image, resulting in a final sample size of 49–53 cells. Image analysis involved selecting regions of interest (ROIs) corresponding to single cells in the same focal plane using ImageJ 1.53t, followed by analysis of mitochondrial network morphology using the StuartLab MiNA tool, as described by Valente et al. (2017), which extracts mitochondrial parameters from segmented mitochondrial structures. The area covered by each region was measured using the Stuart lab MiNA tool in ImageJ, and all values were normalized to their ROI area and the control value. The parameters measured were the mitochondrial footprint, branch length mean, and network branches mean. The mitochondrial footprint represents the area of the image occupied by the mitochondrial signal. The branch length mean is the average length of all the lines used to depict the mitochondrial structures. The network branches mean is the average number of confirmed lines per network structure.

2.5.3. Visualization of the LDPE ROS production

To visualize the ROS production, $LDPE_{<50}$ was incubated with Milli-Q water, ASA, ASA minus glucose, or a glucose suspension with the same concentrations as the ASA for 30 min at 37 ºC. The samples were subsequently incubated with CellROX™ Orange Reagent (Invitrogen™, Thermo Fisher Scientific) according to the manufacturer's instructions. The samples were imaged using an 8-well Ibidi chamber (Ibidi GmbH) in a CLSM (LSM900, Zeiss, Zaventem, Belgium) equipped with high-power diode lasers at 405, 488, 514, and 633 nm, mounted on an inverted laser-scanning microscope (Axio Observer Z1/7, Zeiss, Zaventem, Belgium). The images were obtained at 40x in brightfield (Ex/Em: 549/574 nm; light source intensity: 32.26%; exposure time:150 ms). Image analysis involved selecting regions of interest (ROIs) for the specific particles (n = 24–47) using ImageJ 1.53t, followed by measuring the mean gray value. The value of the control of each condition was subtracted from the values.

2.6. Statistical analysis

All the measurements were normalized to their respective controls. The statistical analyses were performed using GraphPad Prism 9.4.0 (GraphPad Software, San Diego, USA) software. Normality and homoscedasticity were tested with the Shapiro-Wilk and Kolmogorov-

Smirnov tests. Data that was normally distributed was analyzed using a one-way analysis of variance (ANOVA) with the Dunnett post hoc test. If the data were not normally or log-normally distributed, they were analyzed using the Kruskal-Wallis test and multiple-comparison tests. The statistically significant differences are represented with * ($p < 0.05$), ** ($p < 0.01$), and *** ($p < 0.001$), and the data are represented with mean ± standard error to the mean (SEM).

3. Results

This study examined how artificial stomach acid alters the physicochemical properties and toxicity of LDPE microplastics. We aimed to identify key ASA-related changes to relate them to identified toxic effects. Given the evidence that redox processes underlie particle-specific toxicity, the ROS-inducing potential of LDPE and a wider range of common plastic particles was included in the characterization.

3.1. Physicochemical characterization

3.1.1. Physical characterization of all MPs

All studied MPs had an irregular shape (Fig. 1A-D, Suppl. Fig. 1A-E). The maximum Feret diameter of the different MPs ranged from 27.54 ± 19.79 μm for PBT to 237.98 ± 254.2 μm for PA. For the minimum Feret diameter, sizes ranged between 17.03 ± 14.27 μm for PET and 87.53 ± 70.23 μm for PA (mean ± SD, Fig. 1D). Two size fractions of LDPE were studied. The $LDPE_{<50}$ fraction had a max Feret diameter of 74.2 ± 34.09 μm and a min Feret diameter of 41.13 ± 16.34 μm. These dimensions were significantly larger than those of the $LDPE_{30–41}$ fraction ($p < 0.001$, Fig. 1A), which are LDPE particles collected after filtration through a 41 μm filter followed by a 30 μm filter. $LDPE_{30–41}$ had a max Feret diameter of 56.71 ± 35.50 μm and a min Feret diameter of 32.86 ± 25.69 μm. After ASA treatment (Fig. 1C), the max Feret diameter significantly increased to 61.1 ± 32.35 μm, while the min Feret diameter (32.0 ± 10.94 μm) showed no significant difference. Notably, 59.5% of the $LDPE_{30–41}$ exceeded the filter pore size range of 30–41 μm in at least one dimension.

3.1.2. Chemical characterization

XRF showed the presence of several metal traces (Al, Fe, Ti, Cu, Pb, Mn, Zn, and Ni, Fig. 1E), with the remaining mass dominated by the polymer matrix (> 99 wt% C_2H_2). GC-MS showed that the LDPE sample contained phthalates, and derivatives from secondary antioxidants such as Tris(2,4-di-tert-butylphenyl) phosphite (Suppl. Table 1).

DSC showed no significant changes in crystallinity between pristine and ASA-treated LDPE particles. The pristine LDPE particles exhibited a degree of crystallinity between 23.1 and 29.5% (95% confidence interval), based on triplicate measurements of the melting enthalpy and assuming 293 J/g as the heat of fusion for 100% crystalline PE. The DSC measurements on the LDPE-ASA particles revealed a melting enthalpy of 68.95 J/g, corresponding to a degree of crystallinity of 23.5% (Suppl. Fig. 2). FTIR spectroscopy showed no major changes in surface oxidation of $LDPE_{<50}$-ASA particles (Suppl. Fig. 3). The carbonyl index, defined as the peak integration between 1650 and 1850 cm^{-1} to the integration between 1390 and 1490 cm^{-1}, was found to vary more between measurements on the same sample than between treatments. FTIR spectra present the characteristic peaks of LDPE (Gulmine et al., 2002). After the ASA treatment of the plastic, the leachate, measured by ICP-AES, showed traces of Al, Fe, Mn, Pb, and Zn (Fig. 1F).

ROS generation was measured by ESR spectroscopy (Suppl. Fig. 4) before and after 30 min of ASA treatment. The height and surface area of the peaks in the ESR spectra reflect the amount of ROS formation, with higher values indicating increased ROS production (Table 1). $LDPE_{<50}$ appeared to induce ROS, regardless of ASA treatment. More specifically, $LDPE_{<50}$ particles formed $OH^{\cdot}$ and $O_2^{\cdot-}$ in Milli-Q, which increased in intensity after ASA treatment (Figs. 3A and 2B). These results were confirmed and complemented by quantification of ROS using CellROX™ Orange Reagent after incubating LDPE in glucose, ASA without glucose, and ASA. These data showed an increase in ROS production after all treatments compared to Milli-Q water (Fig. 5C). Also, for other particles, such as $LDPE_{50–250,black}$, $LDPE_{50–100,white}$, PMMA, PET, PP, and PVC, ROS formation was observed with ESR after ASA treatment. The strongest ROS production was observed for the different LDPE microplastics, followed by PMMA. No ROS or other radical signal was detected for PBT, neither in Milli-Q nor in ASA. All conditions were normalized to their respective controls, as ASA itself increased ROS formation as well (data not shown).

Because of possible interference, all ESR experiments with $LDPE_{30–41}$ were conducted in ASA, which was stored in a glass (ASAg) or a plastic (ASAp) container. ROS formation was similar in both conditions, except for the surface height after 60 min treatment in LDPE-ASAp (Fig. 5A-B). The ESR spectroscopy results exhibited considerable variability, and data analysis did not reveal statistically significant increased ROS formation compared to their respective controls or between ASAp and ASAg.

3.2. Cellular uptake of $LDPE_{30–41}$ and $LDPE_{30–41}$-ASA microplastics

After a 24 h of exposure, both $LDPE_{30–41}$ and $LDPE_{30–41}$-ASA sedimented onto the cell layer (Fig. 2). Confocal laser scanning microscopy (CLSM) z-stack analysis showed no evidence of particle uptake by Caco−2 cells under any condition. LDPE particles remained extracellularly located, with no signal detected within the cytoplasm or nuclear region of Caco−2 cells. All observed $LDPE_{30–41}$ particles (100%) were either in close proximity to or in contact with the cell membrane. In contrast, 75% of the observed $LDPE_{30–41}$-ASA particles were in contact or close proximity to the cell membrane, while the remaining 25% suspended above the cell monolayer at an average distance of 18.0 ± 2.87 μm from the apical cell membrane.

3.3. Evaluation of cytotoxicity after $LDPE_{30–41}$ and $LDPE_{30–41}$-ASA exposure in Caco−2 cells

Membrane integrity measured by 5-CFDA, AM decreased, even without identified uptake. After a 24 h exposure, both materials induced a concentration-dependent decrease, to 83.86 ± 1.06% for $LDPE_{30–41}$ and 82.36 ± 3.31% for $LDPE_{30–41}$-ASA. $LDPE_{30–41}$ induced subcytotoxic effects across all tested concentrations (1–150 μg/ml), whereas $LDPE_{30–41}$-ASA induced effects only within the concentration range of 25–150 μg/ml (Fig. 3).

Mitochondrial network dynamics were also affected, as the mitochondrial footprint (Fig. 4A) and network branches (Fig. 4C) increased significantly following an exposure to 100 μg/ml $LDPE_{30–41}$-ASA ($p < 0.001$ and $p < 0.05$, respectively). The branch length mean (Fig. 4B) increased following exposure to 10 μg/ml $LDPE_{30–41}$ ($p < 0.05$), 100 μg/ml $LDPE_{30–41}$-ASA ($p < 0.001$), and ASA ($p < 0.05$).

$LDPE_{30–41}$ had a lower mitochondrial footprint than $LDPE_{30–41}$-ASA at 10 and 100 μg/ml ($p < 0.001$). $LDPE_{30–41}$ also had a lower mean branch length than $LDPE_{30–41}$-ASA at 100 μg/ml ($p < 0.01$), but the variability in the $LDPE_{30–41}$ data was greater than this difference. Representative images (Fig. 4D) showed dose-dependent changes in fluorescence that were not supported by quantitative analysis.

4. Discussion

Microplastics (MPs) are a growing concern for both environmental and human health, and have become the focus of many toxicological studies. Alongside important new insights, recent advances have also raised new questions, particularly as most *in vitro* studies rely on commercially available MP beads that poorly reflect environmentally relevant MPs. Manufactured MPs typically have uniform shapes, smooth surfaces, and narrow size ranges, failing to capture the diversity of real-world microplastics, especially for larger and irregular particles. To

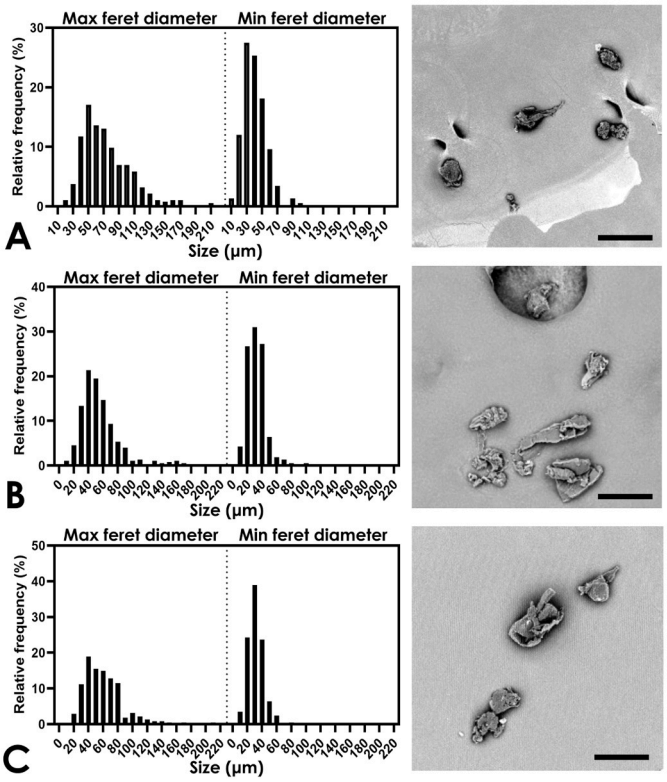

D

Measurement		Mean (µm)	SEM (µm)
$LDPE_{<50}$	Max	74.53	1.11
	Min	41.13	1.54
$LDPE_{30-41}$	Max	56.71	0.25
	Min	32.87	0.63
$LDPE_{30-41}$-ASAg	Max	61.05	1.39
	Min	32.04	1.08
PVC	Max	53.80	3.061
	Min	34.55	2.03
PP	Max	138.01	6.62
	Min	75.89	3.81
PBT	Max	27.54	1.40
	Min	17.58	0.99
PA	Max	237.98	17.98
	Min	87.53	4.97
PET	Max	31.62	1.83
	Min	17.03	1.01

E

Analyte	Result (%)	Std.Dev. (%)	Line	Intensity
SiO_2	0.504	0.007	Si Kα	2.6630
Al_2O_3	0.104	0.004	Al Kα	0.2875
Fe_2O_3	0.048	0.000	Fe Kα	57.2300
CaO	0.032	0.001	Ca Kα	1.6182
K_2O	0.029	0.001	K Kα	0.3390
P_2O_5	0.021	0.002	P Kα	0.1871
SO_3	0.010	0.001	S Kα	0.1966
TiO_2	0.008	0.001	Ti Kα	1.9448
Cl	0.005	0.001	Cl Kα	0.0171
CuO	0.003	0.000	Cu Kα	7.9948
SnO_2	0.002	0.000	Sn Kα	1.3005
PbO	0.002	0.000	Pb $L\beta_1$	4.9364
Cr_2O_3	0.001	0.000	Cr Kα	0.8584
MnO	0.001	0.000	Mn Kα	1.2053
ZnO	0.001	0.000	Zn Kα	3.4447
NiO	0.001	0.000	Ni Kα	1.8009
C_2H_2	99.228	-	-	-

F

Element	$LDPE_{<50}$	ASA
Unit	mg/l	mg/l
Al	1.731	< 0.1
Ba	0.073	< 0.05
Bi	< 0.25	< 0.5
Ca	104.2	67
Cd	< 0.05	0.117
Co	< 0.025	< 0.1
Cr	< 0.025	< 0.1
Cu	0.63	0.662
Fe	0.56	< 0.1
K	436	408
Li	0.13	0.327
Mg	2.24	0.124
Mn	0.34	< 0.05
Na	2593	2062
Ni	0.07	< 0.1
Pb	2.63	< 0.5
Sr	1.26	1.105
Zn	0.75	< 0.1
Ag	< 0.025	< 0.5

Fig. 1. MPs characterization. **A**: size distribution and representative image of $LDPE_{<50}$. **B**: size distribution and representative image of $LDPE_{30–41}$. **C**: size distribution and representative image of $LDPE_{30–41}$-ASA, which is the $LDPE_{30–41}$ fraction treated with ASA for 30 min. (**A-C**) Bars represent the relative frequency (%). All the scale bars are 100 µm. **D**: summary of mean ± SD of the sizes of the maximum and minimum Feret diameter of LDPE, PVC, PP, PBT, PE, and PET). Feret distances were measured using ImageJ (n = 375 for LDPE and n = 200 for PVC, PP, PBT, PE, and PET). **E**: XRF quantitative data of the composition of $LDPE_{<50}$. **F**: ICP results of the ASA and the leachate of $LDPE_{<50}$ after being exposed to ASA for 30 min at 40 ºC.

Table 1
Ranking of microplastic types based on ESR measurement values of the second DMPO-OH peak after 30 min incubation in ASAg or Milli-Q water.

		Plastic incubated for 30 min in ASA		Plastic in Milli-Q	
Rank	**Plastic type**	**2nd Peak Height DMPO˙OH signal (x10 ³)**	**2nd Peak Surface DMPO˙OH signal (x10⁶)**	**2nd Peak Height DMPO˙OH signal (x10 ³)**	**2nd Peak surface DMPO˙OH signal (x10⁶)**
1	$LDPE_{<50}$	16	88	11	51
2	$LDPE_{50-250}$, black	15	21.74	No radical signal observed	
3	$LDPE_{50-100}$, white	12	22.08	No radical signal observed	
4	PMMA (6 μm, white)	11	20.13	No radical signal observed	
5	PET (blue)	10	16.04	No radical signal detected	
6	PP (purple)	10	14.86	No radical signal detected	
7	PVC (white)	10	13.63	No radical signal detected	
8	PBT (white)	No radical signal detected			

address these research gaps, our study investigated pristine and ASA-treated plastics in a commonly used *in vitro* intestinal model (Caco−2 cell line) using a variety of assays to characterize the plastics and assess their potential cytotoxic effects. While our findings establish associations between particle properties and cellular responses, the inherent heterogeneity of environmentally relevant MPs remains an important challenge and likely contributes to inconsistencies across studies. The present study, therefore, represents a first step toward disentangling this variability through a simplified, stepwise approach linking specific physicochemical changes induced by gastric chemical weathering to biological responses.

Contrary to common assumptions, our findings suggest that cytotoxicity can be induced without particle uptake. Both pristine and ASA-treated $LDPE_{30–41}$ particles were larger than most cells and were not taken up by Caco−2 cells, as confirmed by confocal laser scanning microscopy (CLSM) z-stack analysis. No intracellular localization of particles was observed under any condition, with particles remaining extracellular or in direct contact with the apical membrane. Despite the lack of uptake, exposure to both particle types reduced cell viability by compromising membrane integrity (5-CFDA, AM). The strongest effects occurred at high, non-realistic concentrations (>10 μg/ml), while at lower concentrations (≤10 μg/ml), a reduction in membrane integrity was observed only for pristine particles (Fig. 3). This suggests that subtle membrane effects may precede detectable viability changes, as other

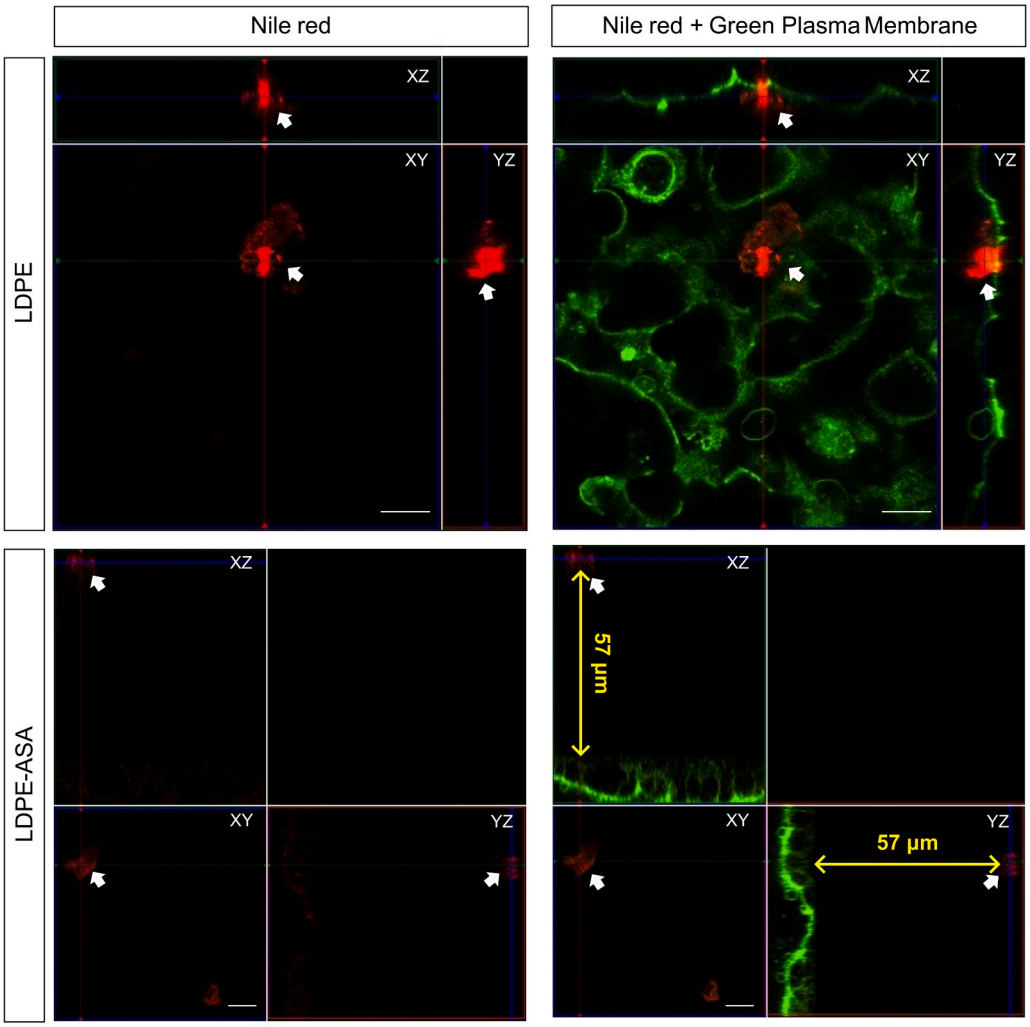

Fig. 2. Uptake and association of $LDPE_{30–41}$ and $LDPE_{30–41}$-ASAg stained with Nile Red in a Caco−2 monolayer. White arrow indicates particles, yellow arrow indicates the distance between the floating $LDPE_{30–41}$-ASA particle and the cellular membrane. Representative XYZ-images of floating and sinked MPs after a 24 h exposure to 100 ug/ml in a confluent Caco−2 monolayer (Membrane - Cellmask Green Plasma membrane stain; Particles - Nile Red). The scale bar is 20 μm.

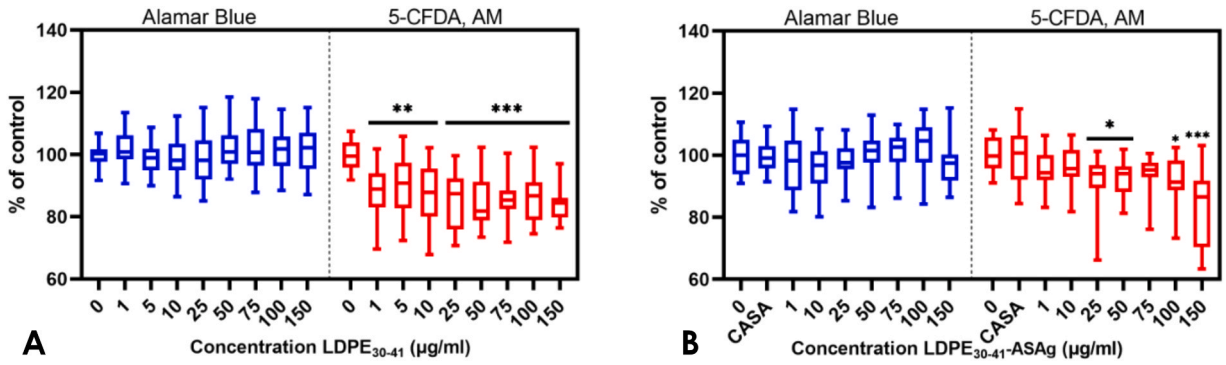

Fig. 3. (Sub-)cytotoxic effects of $LDPE_{30–41}$ and $LDPE_{30–41}$-ASA in a Caco−2 monolayer. Metabolic activity was determined by Alamar Blue, and membrane integrity by 5-CFDA, AM. **A**: Cytotoxic effects of LDPE. **B**: cytotoxic effects of LDPE incubated in ASA. Data represent the percentage of metabolic activity (Alamar Blue) or membrane integrity (5-CFDA, AM) ± standard error to the mean (SEM) relative to control (4 independent experiments, n = 24 for AB and n = 20/16 for 5-CFDA, AM). Box-plot representations show the median (line), interquartile range (box limits), and maximum and minimum values (whiskers). Statistical significance was assessed by one-way ANOVA with control using Dunnett's method if the distribution was normal. If not, a paired *t*-test was applied to the data set. * $p < 0.05$, ** $p < 0.01$, *** $p < 0.001$.

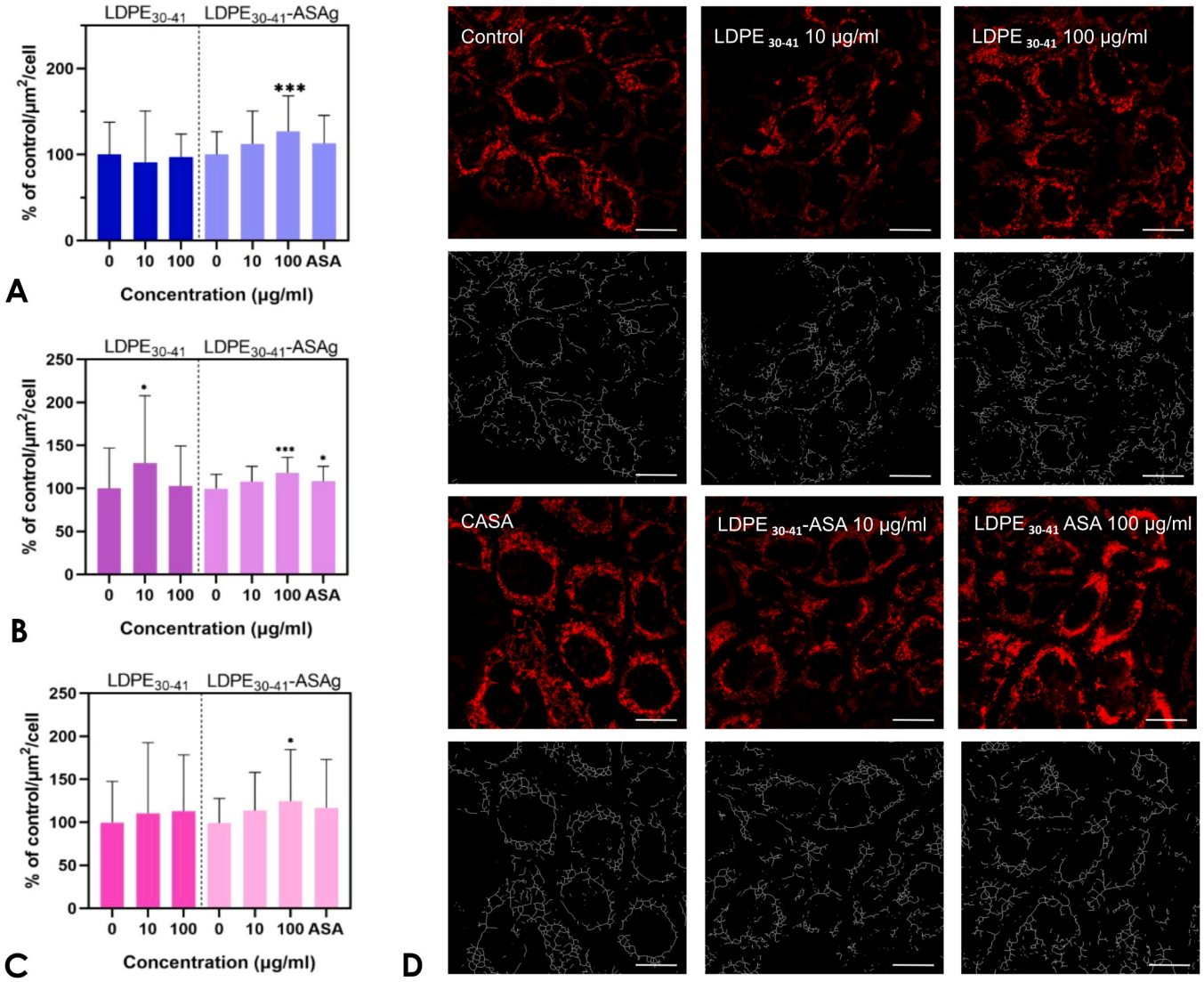

Fig. 4. Effects of LDPE particles on a Caco−2 monolayer mitochondria after 24 h of exposure to 10 or 100 ug/ml of $LDPE_{30–41}$ or $LDPE_{30–41}$-ASA. **A**: Mitochondrial footprint. **B**: Branch length mean. **C**: Network branches mean. **D**: representative images of the different conditions with Mitotracker Red CMXRos and the corresponding skeleton obtained using the MINA tool in Fiji according to Valente et al. (2017). The graphs present the average relative to control ± SEM (n = 9–12 from 3 independent experiments). The scale bar of all the images is 15 µm. Statistical significance was assessed by a paired *t*-test. * $p < 0.05$, ** $p < 0.01$, *** $p < 0.001$.

studies report no strong viability loss at low concentrations across various particles and cell lines (Fournier et al., 2023; Gautam et al., 2022; Goodman et al., 2022; Park et al., 2023; Stock et al., 2019). In the absence of internalization, membrane damage is likely mediated by a combination of mechanical and oxidative processes occurring at the particle–cell interface. Adsorbed microplastic particles can mechanically stretch lipid bilayers and destabilize membrane integrity without requiring oxidative or inflammatory pathways (Fleury and Baulin, 2021). In parallel, MP-induced ROS formation may promote lipid peroxidation of membrane phospholipids, which is increasingly recognized as a central downstream event of oxidative stress (Hu and Palić, 2020; Zhang et al., 2021; Li et al., 2023), leading to loss of membrane integrity and cell viability (Cui et al., 2025; Li et al., 2023). These findings suggest that, for larger MPs, extracellular mechanisms may play a more significant role than intracellular accumulation in mediating intestinal effects. Because ASA exposure altered particle sedimentation behavior, we explored whether differences in particle–cell contact could contribute to the observed effects. Approximately 25% of ASA-weathered particles remained afloat, whereas all pristine LDPE30–41 particles sedimented onto the cell layer (Fig. 2). This may reflect ASA-induced changes in particle surface properties, such as ζ-potential, protein corona formation, or density (Lin et al., 2023; Reznickova et al., 2015), which could influence particle settling and cellular contact (Fischer et al., 2004; McKeen, 2013; Suppl. Table 2). However, due to the size and floatability of the studied LDPE particles, these parameters could not be experimentally determined with the currently available methodologies and therefore remain hypothetical.

We subsequently compared the cytotoxicity of pristine and ASA-weathered particles, building on previous findings showing that mitochondrial dynamics are altered under micro- and nanoplastic (MNP) exposure (Das, 2023; Lee et al., 2022; Saenen et al., 2023). High concentrations of ASA-treated LDPE induced increased mitochondrial fusion, elongated branch length, and an expanded mitochondrial footprint (Fig. 4), which is consistent with an early adaptive response to oxidative stress (Tilokani et al., 2018; Youle and van der Bliek, 2012; Archer, 2013). These changes can temporarily preserve mitochondrial function by sustaining ATP production and maintaining membrane potential (Tilokani et al., 2018; Valente et al., 2017). However, sustained fusion may also reflect impaired mitochondrial fission and mitochondrial turnover, compromising quality control via mitophagy, leading to an accumulation of dysfunctional mitochondria and contributing to cell death. Such dysregulation has been associated with altered metabolic flexibility and reduced capacity to maintain barrier integrity (Huang et al., 2024; Wu et al., 2019). As mitochondria operate as a redox-sensitive network that dynamically responds to cellular oxidative status (Tilokani et al., 2018; Valente et al., 2017; Kuznetsov et al., 2022; Wang et al., 2022; Wu et al., 2019), and given the observed mitochondrial alterations in the absence of particle uptake, the cellular redox potential of the particles was further investigated (Banerjee and Shelver, 2021; Hu and Palić, 2020) using ESR and CellROX Orange Reagent. Both pristine and ASA-treated LDPE particles increased ROS levels in a non-cellular environment, with stronger effects after ASA treatment (Fig. 5). We hypothesize that the increased ROS production is driven by trace amounts of metals, likely originating from plastic production and handling (Suppl. Table 1), as redox activity is known to be enhanced by high surface area, functional groups, and transition metals on particle surfaces (Gao et al., 2022; Hu and Palić, 2020; Xu et al., 2024), despite only minimal surface oxidation as indicated by the carbonyl index. In addition, glucose in the artificial stomach acid may further promote ROS formation via metal-catalyzed autooxidation in the presence of trace Fe (0.5 ppm) detected in the leachate (Chikezie et al., 2015). These results support a model in which pristine MPs primarily induce membrane damage through direct physical interactions, whereas ASA-treated MPs may additionally contribute to cellular effects via leachate-associated and redox-mediated effects. Importantly, while mitochondrial network and ROS alterations were directly observed, the link to particle surface modifications remains to be validated experimentally.

To conceptually demonstrate the increase in redox-inducing potential after ASA treatment, we conducted a screening to assess the ROS-inducing potential of LDPE and other irregular MPs found in everyday products (De Vos et al., 2021; Shakiba et al., 2021; Shen and Worrell, 2014). This showed LDPE as the plastic with the highest ROS-inducing potential, but other plastics also showed increased redox potential after ASA treatment, validating our previous findings (Table 1) and aligning with previous studies (Duan et al., 2022). Hu and Palić (2020) demonstrated that UV-weathered particles trigger ROS production and oxidative stress, leading to cellular damage, and Krasucka et al. (2022) further found that *in vitro* digestive or environmental processes modify particle surfaces, thereby influencing toxicity. This study acknowledges the limitations of its design and includes control experiments to eliminate potential artifacts. To address the interaction between nanoparticles and assay readouts (Andraos et al., 2020), we assessed potential particle interference with all fluorescent assays using a plate reader and confocal microscopy, which was minimal (Suppl. Fig. 5). In addition, we faced a higher variability in responses due to the heterogeneous size and distribution of the MP suspensions, necessitating the use of multiple independent experiments and complementary assays. Despite this approach, ESR measurements showed considerable

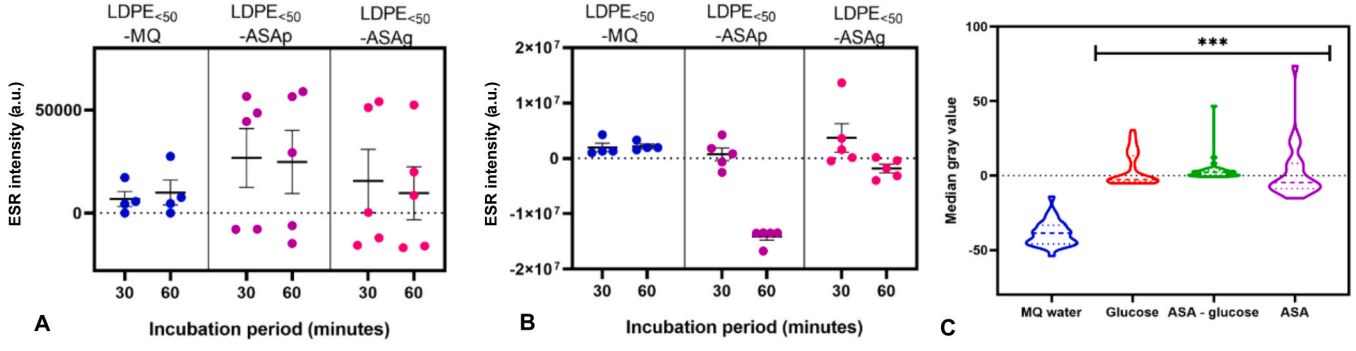

Fig. 5. Quantification of the ESR spectroscopy measurements of the second DMPO·OH peak (in arbitrary units), and ROS formation measurements with CellROX Orange Reagent. **A:** Summary of the height of the second peak minus their respective controls of LDPE$_{<50}$ in MilliQ water (LDPE$_{<50}$-MQ), LDPE$_{<50}$ incubated in ASA stored in plastic (LDPE$_{<50}$-ASAp), and LDPE$_{<50}$ incubated in ASA stored in glass (LDPE$_{<50}$-ASAg). **B:** Summary of the surface of the second peak minus their respective controls of LDPE$_{<50}$-MQ, LDPE$_{<50}$-ASAp, and LDPE$_{<50}$-ASAg. **C:** summary of the median gray value of CellROX Orange Reagent intensity of individual particles minus their respective controls of LDPE$_{<50}$ in MilliQ water (MQ water), LDPE$_{<50}$ incubated in ASA (ASA), LDPE$_{<50}$ incubated in ASA without glucose (ASA - glucose), and LDPE$_{<50}$ incubated in glucose (Glucose). The summary data Graphs A and B represent individual single values (dots), average and SEM, and Graph C represents a violin plot with median (dotted line) and quartiles (line). Statistical significance was assessed by one-way ANOVA with control using Dunnett's method if the distribution was normal. If not, the Wilcoxon test was applied to the data set. *** $p < 0.001$.

variability, likely reflecting the high sensitivity of the technique to heterogeneous samples (Davies, 2016). Therefore, findings were interpreted alongside results from other assays and validated across different plastic types to strengthen their robustness. We do have to note that, due to the sensitivity of the equipment, chemical analyses required plastic amounts 33–330 times higher than those used in cell-based experiments. The simplified ASA weathering model and Caco−2 cell system can also be considered as limitations, although they were deliberately selected to provide a controlled and reproducible framework for identifying specific physicochemical changes and their biological consequences. A limitation of our ASA model is that it focuses solely on chemical gastric weathering during a 30-min exposure, which is primarily representative of liquid digestion and does not capture the full complexity of gastrointestinal processes. Similarly, while the widely used Caco−2 model facilitates comparison with existing studies, it does not fully reproduce the intestinal epithelium in vivo. Nevertheless, the insights gained from this study provide a foundation for future experiments incorporating more complex digestion models and advanced intestinal systems in a stepwise manner (Bredeck et al., 2022). By systematically addressing key sources of variability and incorporating thorough microplastic characterization, we advance our understanding of the potential health impacts of microplastics and provide insights that support the development of safer polymer materials.

5. Conclusions

Our study demonstrated that fragment-shaped LDPE MPs can negatively affect Caco−2 cells, even in the absence of detectable cellular uptake. Exposure to a simplified artificial stomach acid model, mimicking human gastric chemical weathering, altered the physicochemical properties of LDPE particles and shifted their toxicity profile. Our data indicated that pristine plastics sediment more readily, being associated with a higher membrane integrity loss, supporting the hypothesis that pristine MPs primarily exert effects through direct particle-cell interaction. In contrast, ASA-treated LDPE showed a higher redox potential, which was a trend in other particles, even though there was variation between polymers. These physicochemical differences translated into downstream effects in mitochondrial network dynamics, possibly linked to the measured metal leaching present in ASA-treated LDPE. While the proposed links require further validation, a key strength of this study is its integration of physicochemical and biological analyses. Extending such combined approaches, particularly under more physiologically relevant conditions and using a more comprehensive digestion model, will be crucial for a better understanding of the effects of real-world plastic particles in future work.

CRediT authorship contribution statement

Inés Tejeda: Writing – original draft, Visualization, Validation, Investigation, Formal analysis, Data curation. **Nelly D. Saenen:** Writing – review & editing, Resources, Investigation, Funding acquisition. **Frank G.A.J. Van Belleghem:** Writing – review & editing, Funding acquisition. **Karen Smeets:** Writing – review & editing, Supervision, Funding acquisition, Conceptualization. **Margo S. Witters:** Writing – review & editing, Investigation. **Wouter Marchal:** Writing – review & editing. **An Hardy:** Writing – review & editing. **Jacco J. Briedé:** Writing – review & editing, Resources.

Funding

This work was supported by the Enabling Technologies Hotels programme within the ZonMw Microplastics & Health (MPH) programme for the project titled "Uptake, Translocation, and Toxicity of Microplastics Isolated from Shellfish in Human Gut Cells" under project number 458001012; Bijzonder Onderzoeksfonds (BOF) UHasselt under Grant R9782; Fonds Wetenschappelijk Onderzoek – Vlaanderen (FWO) under Grant 1258725 N (assigned to Nelly Saenen); and European Marine Biological Resource Centre (EMBRC) Belgium under GOH3817N.

Declaration of Competing Interest

The authors declare that they have no known competing financial interests or personal relationships that could have appeared to influence the work reported in this paper.

Acknowledgements

We thank Ir. Gianfabio Mangione, Ir. Thomas Vranken and Natascha Steffanie for their skillful support and technical assistance. Ria Vanderspikken is thanked for the administrative assistance.

Appendix A. Supporting information

Supplementary data associated with this article can be found in the online version at doi:10.1016/j.ecoenv.2026.120532.

Data availability

Data will be made available on request.

References

Alimi, O.S., Claveau-Mallet, D., Kurusu, R.S., Lapointe, M., Bayen, S., Tufenkji, N., 2022. Weathering pathways and protocols for environmentally relevant microplastics and nanoplastics: what are we missing? J. Hazard. Mater. 423, 126955. https://doi.org/10.1016/j.jhazmat.2021.126955.

Andraos, C., Yu, I.J., Gulumian, M., 2020. Interference: a much-neglected aspect in high-throughput screening of nanoparticles. Int. J. Toxicol. 39 (5), 397–421. https://doi.org/10.1177/1091581820938335.

Angelis, I.D., Turco, L., 2011. Caco-2 cells as a model for intestinal absorption, 20.6.1-20.6.15 Curr. Protoc. Toxicol. 47 (1). https://doi.org/10.1002/0471140856.tx2006s47.

Archer, S.L., 2013. Mitochondrial dynamics—Mitochondrial fission and fusion in human diseases. New. Engl. J. Med. 369 (23), 2236–2251. https://doi.org/10.1056/NEJMra1215233.

Banerjee, A., Shelver, W.L., 2021. Micro- and nanoplastic induced cellular toxicity in mammals: a review. Sci. Total. Environ. 755, 142518. https://doi.org/10.1016/j.scitotenv.2020.142518.

Barboza, L.G.A., Cózar, A., Gimenez, B.C.G., Barros, T.L., Kershaw, P.J., Guilhermino, L., 2019. Chapter 17—Macroplastics Pollution in the Marine Environment. In. In: Sheppard, C. (Ed.), World Seas: An Environmental Evaluation (Second Edition). Academic Press, pp. 305–328. https://doi.org/10.1016/B978-0-12-805052-1.00019-X.

Barboza, L.G.A., Dick Vethaak, A., Lavorante, B.R.B.O., Lundebye, A.-K., Guilhermino, L., 2018. Marine microplastic debris: an emerging issue for food security, food safety, and human health. Mar. Pollut. Bull. 133, 336–348. https://doi.org/10.1016/j.marpolbul.2018.05.047.

Bond, T., Morton, J., Al-Rekabi, Z., Cant, D., Davidson, S., Pei, Y., 2022. Surface properties and rising velocities of pristine and weathered plastic pellets. Environ. Sci. Process. Impacts 24 (5), 794–804. https://doi.org/10.1039/D1EM00495F.

Bredeck, G., Halamoda-Kenzaoui, B., Bogni, A., Lipsa, D., Bremer-Hoffmann, S., 2022. Tiered testing of micro- and nanoplastics using intestinal in vitro models to support hazard assessments. Environ. Int. 158, 106921. https://doi.org/10.1016/j.envint.2021.106921.

Briske-Anderson, M.J., Finley, J.W., Newman, S.M., 1997. The influence of culture time and passage number on the morphological and physiological development of Caco-2 cells. Proc. Soc. Exp. Biol. Med. Soc. Exp. Biol. Med. 214 (3), 248–257. https://doi.org/10.3181/00379727-214-44093.

Chikezie, P., Ojiako, O., Ogbuji, A., 2015. Oxidative Stress in Diabetes Mellitus. Int. J. Biol. Chem. 9 (3), 92–109. https://doi.org/10.17311/ijbc.2015.92.109.

Cui, C., Guo, Z., Liu, Y., Han, N., Song, J., Chen, Y., Zheng, Y., Sheng, C., Balmer, L., Li, H., Liu, R., Liu, L., Du, J., Wu, Z., 2025. Tissue-specific distribution of microplastics in human blood and carotid plaques: a paired sample analysis. Environ. Int. 203, 109743. https://doi.org/10.1016/j.envint.2025.109743.

Das, A., 2023. The emerging role of microplastics in systemic toxicity: involvement of reactive oxygen species (ROS). Sci. Total. Environ. 895, 165076. https://doi.org/10.1016/j.scitotenv.2023.165076.

Davies, M.J., 2016. Detection and characterisation of radicals using electron paramagnetic resonance (EPR) spin trapping and related methods. Methods Curr. Methods Unravel React. Oxyg. Species (ROS) Biol. 109, 21–30. https://doi.org/10.1016/j.ymeth.2016.05.013.

De Vos, L., Van de Voorde, B., Van Daele, L., Dubruel, P., Van Vlierberghe, S., 2021. Poly (alkylene terephthalate)s: From current developments in synthetic strategies towards

applications. Eur. Polym. J. 161, 110840. https://doi.org/10.1016/j.eurpolymj.2021.110840.
Duan, J., Li, Y., Gao, J., Cao, R., Shang, E., Zhang, W., 2022. ROS-mediated photoaging pathways of nano- and micro-plastic particles under UV irradiation. Water Res. 216, 118320. https://doi.org/10.1016/j.watres.2022.118320.
Dusza, H., Katrukha, E., Nijmeijer, S., Akhmanova, A., Vethaak, A., Walker, D., Legler, J., 2022. Uptake, transport, and toxicity of pristine and weathered micro- and nanoplastics in human placenta cells. Environ. Health Perspect. 130, 97006. https://doi.org/10.1289/EHP10873.
EFSA's Scientific Committee promotes alternatives to animal testing | EFSA. (2009, June 8). https://www.efsa.europa.eu/en/news/efsas-scientific-committee-promotes-alternatives-animal-testing.
El-Sherif, D.M., Eloffy, M.G., Elmesery, A., Abouzid, M., Gad, M., El-Seedi, H.R., Brinkmann, M., Wang, K., Al Naggar, Y., 2022. Environmental risk, toxicity, and biodegradation of polyethylene: A review. Environ. Sci. Pollut. Res. 29 (54), 81166–81182. https://doi.org/10.1007/s11356-022-23382-1.
Emblem, A., 2012. Plastic properties for packaging materials. In: Packaging Technology, 1. Elsevier, pp. 287–309. https://doi.org/10.1533/9780857095701.2.287.
European Parliament & Council of the European Union, 2006. Regulation (EC) No 1907/2006 (REACH). Off. J. Eur. Union. L396, 1–849. https://eur-lex.europa.eu/legal-content/EN/TXT/?uri=CELEX:32006R1907.
Ferreira, R.O.G., Nag, R., Gowen, A., Xu, J.-L., 2024. Deciphering the cytotoxicity of micro- and nanoplastics in Caco-2 cells through meta-analysis and machine learning. Environ. Pollut. 362, 124971. https://doi.org/10.1016/j.envpol.2024.124971.
Fischer, H., Polikarpov, I., Craievich, A.F., 2004. Average protein density is a molecular-weight-dependent function. Protein Science A Publication Protein Society 13 (10), 2825–2828. https://doi.org/10.1110/ps.04688204.
Fleury, J.-B., Baulin, V.A., 2021. Microplastics destabilize lipid membranes by mechanical stretching. Proc. Natl. Acad. Sci. 118 (31), e2104610118. https://doi.org/10.1073/pnas.2104610118.
Fournier, E., Étienne-Mesmin, L., Grootaert, C., Jelsbak, L., Syberg, K., Blanquet-Diot, S., Mercier-Bonin, M., 2021. Microplastics in the human digestive environment: A focus on the potential and challenges facing in vitro gut model development. J. Hazard. Mater. 415, 125632. https://doi.org/10.1016/j.jhazmat.2021.125632.
Fournier, E., Leveque, M., Ruiz, P., Ratel, J., Durif, C., Chalancon, S., Amiard, F., Edely, M., Bezirard, V., Gaultier, E., Lamas, B., Houdeau, E., Lagarde, F., Engel, E., Etienne-Mesmin, L., Blanquet-Diot, S., Mercier-Bonin, M., 2023. Microplastics: What happens in the human digestive tract? First evidences in adults using in vitro gut models. J. Hazard. Mater. 442, 130010. https://doi.org/10.1016/j.jhazmat.2022.130010.
Gao, Z., Chou, P.I., Liu, J., Zhu, Y., Jun, Y.S., 2022. Oxidative roles of polystyrene-based nanoplastics in inducing manganese oxide formation under light illumination. ACS Nano 16 (12), 20238–20250. https://doi.org/10.1021/acsnano.2c05803.
Gautam, R., Jo, J., Acharya, M., Maharjan, A., Lee, D., K.C., P.B., Kim, C., Kim, K., Kim, H., Heo, Y., 2022. Evaluation of potential toxicity of polyethylene microplastics on human derived cell lines. Sci. Total. Environ. 838, 156089. https://doi.org/10.1016/j.scitotenv.2022.156089.
Geyer, R., Jambeck, J.R., Law, K.L., 2017. Production, use, and fate of all plastics ever made (Scopus). Sci. Adv. 3 (7). https://doi.org/10.1126/sciadv.1700782.
Goodman, K.E., Hua, T., Sang, Q.-X.A., 2022. Effects of Polystyrene Microplastics on Human Kidney and Liver Cell Morphology, Cellular Proliferation, and Metabolism. ACS Omega 7 (38), 34136–34153. https://doi.org/10.1021/acsomega.2c03453.
Gulmine, J.V., Janissek, P.R., Heise, H.M., Akcelrud, L., 2002. Polyethylene characterization by FTIR. Polym. Test. 21 (5), 557–563. https://doi.org/10.1016/S0142-9418(01)00124-6.
Hartmann, N.B., Hüffer, T., Thompson, R.C., Hassellöv, M., Verschoor, A., Daugaard, A.E., Rist, S., Karlsson, T., Brennholt, N., Cole, M., Herrling, M.P., Hess, M.C., Ivleva, N.P., Lusher, A.L., Wagner, M., 2019. Are We Speaking the Same Language? Recommendations for a Definition and Categorization Framework for Plastic Debris. Environ. Sci. & Technol. 53 (3), 1039–1047. https://doi.org/10.1021/acs.est.8b05297.
Hirt, N., Body-Malapel, M., 2020. Immunotoxicity and intestinal effects of nano- and microplastics: A review of the literature. Part. Fibre Toxicol. 17, 57. https://doi.org/10.1186/s12989-020-00387-7.
Ho, Y.-W., Lim, J.Y., Yeoh, Y.K., Chiou, J.-C., Zhu, Y., Lai, K.P., Li, L., Chan, P.K.S., Fang, J.K.-H., 2022. Preliminary Findings of the High Quantity of Microplastics in Faeces of Hong Kong Residents. Toxics 10 (8), 414. https://doi.org/10.3390/toxics10080414.
Hu, M., Palić, D., 2020. Micro- and nano-plastics activation of oxidative and inflammatory adverse outcome pathways. Redox Biol. 37, 101620. https://doi.org/10.1016/j.redox.2020.101620.
Huang, J.Y.L., Ingyu, Lee, Feng, C., Kim, Hyunook, Chin-Pao, 2024. Electrophoresis characterization of nanoplastic particle surface charge in dilute aqueous electrolytes—Jui-Yen Lin, Ingyu Lee, Cuijuan Feng, Hyunook Kim, Chin-Pao Huang, 2024. Environ. Eng. Sci. https://journals.sagepub.com/doi/10.1089/ees.2024.0076?utm_source=chatgpt.com.
Kennedy, M.S., Chang, E.B., 2020. The microbiome: Composition and locations. Progress. Mol. Biol. Transl. Sci. 176, 1–42. https://doi.org/10.1016/bs.pmbts.2020.08.013.
Kershaw, P.J., Rochman, C.M., 2015. Sources fate Eff. Micro Mar. Environ. Part. 2 a Glob. Assess. Rep. Stud. -IMO/FAO/UNESCO-IOC/WMO/IAEA/UN/UNEP Jt. Group. Experts Sci. Asp. Mar. Environ. Prot. (GESAMP) Eng. No. 93.
Kosuth, M., Mason, S.A., Wattenberg, E.V., 2018. Anthropogenic contamination of tap water, beer, and sea salt. PloS. One 13 (4), e0194970. https://doi.org/10.1371/journal.pone.0194970.
Krasucka, P., Bogusz, A., Baranowska-Wójcik, E., Czech, B., Szwajgier, D., Rek, M., Ok, Y.S., Oleszczuk, P., 2022. Digestion of plastics using in vitro human gastrointestinal tract and their potential to adsorb emerging organic pollutants. Sci. Total. Environ. 843, 157108. https://doi.org/10.1016/j.scitotenv.2022.157108.
Kus, M., Ibragimow, I., Piotrowska-Kempisty, H., 2023. Caco-2 cell line standardization with pharmaceutical requirements and in vitro model suitability for permeability assays. Pharmaceutics 15 (11), 2523. https://doi.org/10.3390/pharmaceutics15112523.
Kuznetsov, A.V., Margreiter, R., Ausserlechner, M.J., Hagenbuchner, J., 2022. The Complex Interplay between Mitochondria, ROS and Entire Cellular Metabolism. Article 10. Antioxidants 11 (10). https://doi.org/10.3390/antiox11101995.
Lee, S.E., Yi, Y., Moon, S., Yoon, H., Park, Y.S., 2022. Impact of Micro- and Nanoplastics on Mitochondria. Metabolites 12 (10), 897. https://doi.org/10.3390/metabo12100897.
Li, Y., Tao, L., Wang, Q., Wang, F., Li, G., Song, M., 2023. Potential Health Impact of Microplastics: A Review of Environmental Distribution, Human Exposure, and Toxic Effects. Environ. & Health 1 (4), 249–257. https://doi.org/10.1021/envhealth.3c00052.
Liebezeit, G., Liebezeit, E., 2013. Non-pollen particulates in honey and sugar. Food Addit. & Contam. Part. A 30 (12), 2136–2140. https://doi.org/10.1080/19440049.2013.843025.
Lin, J.Y., Lee, I., Tzeng, J.H., Li, W., Kim, H., Huang, C.-P., 2023. The surface acidity of freshly synthesized microplastics particles in simple electrolyte. Colloids Surf. A Physicochem. Eng. Asp. 675, 132000. https://doi.org/10.1016/j.colsurfa.2023.132000.
Liu, G., Jiang, Q., Qin, L., Zeng, Z., Zhang, P., Feng, B., Liu, X., Qing, Z., Qing, T., 2024. The influence of digestive tract protein on cytotoxicity of polyvinyl chloride microplastics. Sci. Total. Environ. 945, 174023. https://doi.org/10.1016/j.scitotenv.2024.174023.
Lyshtva, P., Torkelis, A., Kobets, Y., Carpio-Vallejo, E., Dobri, A., Barbir, J., Voronova, V., Denafas, G., Kliucininkas, L., 2025. Characterization of the municipal plastic and multilayer packaging waste in three cities of the Baltic States. Sustainability 17 (3), 986. https://doi.org/10.3390/su17030986.
McKeen, L.W., 2013. 1—Introduction to Use of Plastics in Food Packaging. In: Ebnesajjad, S. (Ed.), Plastic Films in Food Packaging. William Andrew Publishing, pp. 1–15. https://doi.org/10.1016/B978-1-4557-3112-1.00001-6.
Park, J.H., Hong, S., Kim, O.H., Kim, C.H., Kim, J., Kim, J.W., Hong, S., Lee, H.J., 2023. Polypropylene microplastics promote metastatic features in human breast cancer. Sci. Rep. 13 (1), 6252. https://doi.org/10.1038/s41598-023-33393-8.
Paul, M.B., Böhmert, L., Thünemann, A.F., Loeschner, K., Givelet, L., Fahrenson, C., Braeuning, A., Sieg, H., 2024. Influence of artificial digestion on characteristics and intestinal cellular effects of micro-, submicro- and nanoplastics. Food Chem. Toxicol. 184, 114423. https://doi.org/10.1016/j.fct.2023.114423.
Prabhu, K., Ghosh, S., Sethulekshmi, S., Shriwastav, A., 2024. vitro digestion of microplastics in human digestive system: Insights into particle morphological changes and chemical leaching. Sci. Total. Environ. 934, 173173. https://doi.org/10.1016/j.scitotenv.2024.173173.
Prata, J.C., da Costa, J.P., Lopes, I., Duarte, A.C., Rocha-Santos, T., 2020. Environmental exposure to microplastics: An overview on possible human health effects. Sci. Total. Environ. 702, 134455. https://doi.org/10.1016/j.scitotenv.2019.134455.
Prata, J.C., Reis, V., Matos, J.T.V., da Costa, J.P., Duarte, A.C., Rocha-Santos, T., 2019. A new approach for routine quantification of microplastics using Nile Red and automated software (MP-VAT). Sci. Total. Environ. 690, 1277–1283. https://doi.org/10.1016/j.scitotenv.2019.07.060.
Qi, Y., Yang, X., Pelaez, A.M., Huerta Lwanga, E., Beriot, N., Gertsen, H., Garbeva, P., Geissen, V., 2018. Macro- and micro- plastics in soil-plant system: Effects of plastic mulch film residues on wheat (Triticum aestivum) growth. Sci. Total Environ. 645 (23), 1048–1056. https://doi.org/10.1016/j.scitotenv.2018.07.229.
Refosco, A., Dierkes, J., Kögel, T., Dankel, S.N., Laupsa-Borge, J., Gomiero, A., Daniel, D.B., 2025. Microplastics in human feces: A pilot study exploring links with dietary habits. Micro Nanoplastics 5 (1), 22. https://doi.org/10.1186/s43591-025-00129-6.
Reznickova, A., Novotna, Z., Kolská, Z., Slepickova Kasalkova, N., Rimpelova, S., Svorcik, V., 2015. Enhanced adherence of mouse fibroblast and vascular cells to plasma modified polyethylene. Materials Science Engineering C 52, 259–266. https://doi.org/10.1016/j.msec.2015.03.052.
Saenen, N.D., Witters, M.S., Hantoro, I., Tejeda, I., Ethirajan, A., Van Belleghem, F., Smeets, K., 2023. Polystyrene Microplastics of Varying Sizes and Shapes Induce Distinct Redox and Mitochondrial Stress Responses in a Caco-2 Monolayer. Article 3. Antioxidants 12 (3). https://doi.org/10.3390/antiox12030739.
Schirmer, K., Chan, A.G.J., Greenberg, B.M., Dixon, D.G., Bols, N.C., 1997. Methodology for demonstrating and measuring the photocytotoxicity of fluoranthene to fish cells in culture. Toxicol. Vitro 11 (1), 107–119. https://doi.org/10.1016/S0887-2333(97)00002-7.
Shakiba, M., Rezvani Ghomi, E., Khosravi, F., Jouybar, S., Bigham, A., Zare, M., Abdouss, M., Moaref, R., Ramakrishna, S., 2021. Nylon—A material introduction and overview for biomedical applications. Polym. Adv. Technol. 32 (9), 3368–3383. https://doi.org/10.1002/pat.5372.
Shen, L., Worrell, E., 2014. Chapter 13—Plastic Recycling. In. In: Worrell, E., Reuter, M. A. (Eds.), Handbook of Recycling. Elsevier, pp. 179–190. https://doi.org/10.1016/B978-0-12-396459-5.00013-1.
Song, Y., Zhang, J., Shen, X., Yang, L., Jia, Y., Song, F., Huang, Y., Han, B., Zhou, S., Zhang, N., Ma, G., 2025. Microplastics in stools and their influencing factors among young adults from three cities in China: A multicenter cross-sectional study. Environ. Pollut. 364, 125168. https://doi.org/10.1016/j.envpol.2024.125168.
Stock, V., Böhmert, L., Lisicki, E., Block, R., Cara-Carmona, J., Pack, L.K., Selb, R., Lichtenstein, D., Voss, L., Henderson, C.J., Zabinsky, E., Sieg, H., Braeuning, A., Lampen, A., 2019. Uptake and effects of orally ingested polystyrene microplastic

particles in vitro and in vivo. Arch. Toxicol. 93 (7), 1817–1833. https://doi.org/10.1007/s00204-019-02478-7.

Tilokani, L., Nagashima, S., Paupe, V., Prudent, J., 2018. Mitochondrial dynamics: Overview of molecular mechanisms. Essays Biochem. 62 (3), 341–360. https://doi.org/10.1042/EBC20170104.

Torkelis, A., Dvarionienė, J., Denafas, G., 2024. The factors influencing the recycling of plastic and composite packaging waste. Sustainability 16 (21), 9515. https://doi.org/10.3390/su16219515.

Valente, A.J., Maddalena, L.A., Robb, E.L., Moradi, F., Stuart, J.A., 2017. A simple ImageJ macro tool for analyzing mitochondrial network morphology in mammalian cell culture. Acta Histochem. 119 (3), 315–326. https://doi.org/10.1016/j.acthis.2017.03.001.

Völkl, M., Jérôme, V., Weig, A., Jasinski, J., Meides, N., Strohriegl, P., Scheibel, T., Freitag, R., 2022. Pristine and artificially-aged polystyrene microplastic particles differ in regard to cellular response. J. Hazard. Mater. 435, 128955. https://doi.org/10.1016/j.jhazmat.2022.128955.

Wang, Z., Ding, J., Razanajatovo, R.M., Huang, J., Zheng, L., Zou, H., Wang, Z., Liu, J., 2022. Sorption of selected pharmaceutical compounds on polyethylene microplastics: Roles of pH, aging, and competitive sorption. Chemosphere 307, 135561. https://doi.org/10.1016/j.chemosphere.2022.135561.

Wu, P., Huang, J., Zheng, Y., Yang, Y., Zhang, Y., He, F., Chen, H., Quan, G., Yan, J., Li, T., Gao, B., 2019. Environmental occurrences, fate, and impacts of microplastics. Ecotoxicol. Environ. Saf. 184, 109612. https://doi.org/10.1016/j.ecoenv.2019.109612.

Xu, Y., Ou, Q., van der Hoek, J.P., Liu, G., Lompe, K.M., 2024. Photo-oxidation of micro- and nanoplastics: Physical, chemical, and biological effects in environments. Environ. Sci. & Technol. 58 (2), 991–1009. https://doi.org/10.1021/acs.est.3c07035.

Youle, R.J., van der Bliek, A.M., 2012. Mitochondrial fission, fusion, and stress. Science 337 (6098), 1062–1065. https://doi.org/10.1126/science.1219855.

Zhang, K., Hamidian, A.H., Tubić, A., Zhang, Y., Fang, J.K.H., Wu, C., Lam, P.K.S., 2021. Understanding plastic degradation and microplastic formation in the environment: A review. Environ. Pollut. 274, 116554. https://doi.org/10.1016/j.envpol.2021.116554.

Ziessman, H.A., Chander, A., Clarke, J.O., Ramos, A., L.Wahl, R., 2009. The added diagnostic value of liquid gastric emptying compared with solid emptying alone. J. Nucl. Med. 50 (5), 726–731. https://doi.org/10.2967/jnumed.108.059790.